Accepted Manuscript

Pyrolysis, kinetics analysis, thermodynamics parameters and reaction mechanism of *Typha latifolia* to evaluate its bioenergy potential

Muhammad Sajjad Ahmad, Muhammad Aamer Mehmood, Syed Taha Haider Taqvi, Ali Elkamel, Chen-Guang Liu, Xujian Ren, Sawsan Abdulaziz Rahimuddin, Munazza Gull

PII: S0960-8524(17)31476-1
DOI: http://dx.doi.org/10.1016/j.biortech.2017.08.162
Reference: BITE 18771

To appear in: *Bioresource Technology*

Received Date: 6 July 2017
Revised Date: 3 August 2017
Accepted Date: 27 August 2017

Please cite this article as: Ahmad, M.S., Mehmood, M.A., Taqvi, S.T.H., Elkamel, A., Liu, C-G., Ren, X., Rahimuddin, S.A., Gull, M., Pyrolysis, kinetics analysis, thermodynamics parameters and reaction mechanism of *Typha latifolia* to evaluate its bioenergy potential, *Bioresource Technology* (2017), doi: http://dx.doi.org/10.1016/j.biortech.2017.08.162

Pyrolysis, kinetics analysis, thermodynamics parameters and reaction mechanism of *Typha latifolia* to evaluate its bioenergy potential

Muhammad Sajjad Ahmad [b,c], Muhammad Aamer Mehmood [a,b]*, Syed Taha Haider Taqvi [c], Ali Elkamel [c], Chen-Guang Liu [d]*, Xujian Ren [d], Sawsan Abdulaziz Rahimuddin [e], Munazza Gull [e]

[a] College of Bioengineering, Sichuan University of Science and Engineering, Zigong-643000, People's Republic of China

[b] Bioenergy Research Center, Department of Bioinformatics and Biotechnology, Government College University Faisalabad, Faisalabad-38000, Pakistan

[c] Chemical Engineering Department, University of Waterloo, Ontario, Canada

[d] State Key Laboratory of Microbial Metabolism, School of Life Sciences and Biotechnology, Shanghai Jiao Tong University, Shanghai, China

[e] Biochemistry Department, Faculty of Science, King Abdulaziz University, Jeddah, 21551, Saudi Arabia

Corresponding authors: MA Mehmood (draamer@gcuf.edu.pk); CG Liu (cg.liu@sjtu.edu.cn)

Abstract

This work was focused on understanding the pyrolysis of *Typha latifolia*. Kinetics, thermodynamics parameters and pyrolysis reaction mechanism were studied using thermogravimetric data. Based on activation energies and conversion points, two regions of pyrolysis were established. Region-I occurred between the conversion rate 0.1 to 0.4 with peak temperatures 538K, 555K, 556K at the heating rates of 10 $Kmin^{-1}$, 30 $Kmin^{-1}$, and 50 $Kmin^{-1}$, respectively. Similarly, the Region-II occurred between 0.4 to 0.8 with peak temperatures of 606K, 621K, 623K at same heating rates. The best model was diffusion mechanism in Region-I. In Region-II, the reaction order was shown to be 2^{nd} and 3^{rd}. The values of activation energy calculated using FWO and KAS methods (134-204 kJ mol^{-1}) remained same in both regions reflecting that the best reaction mechanism was predicted. Kinetics and thermodynamic parameters including E, ΔH, ΔS, ΔG shown that *T. latifolia* biomass is a remarkable feedstock for bioenergy.

Keywords: *Typha latifolia*; thermogravimetric study; reaction mechanism; bioenergy; low-cost biomass

1. Introduction

At present, energy requirements of the world are met through fossil fuels. Owing to their non-renewable nature, fossil fuel deposits may be completely exhausted from Earth in 70 years from now. Alternatively, biomass is believed to be a reliable future energy source along with solar, wind and hydrothermal. Among all the energy resources worldwide, biomass provides up to 10 %, with an annual increase of 2.5% (Edrisi and Abhilash, 2016). In the USA and Brazil, almost 80 percent of the fuel comes from renewables, specifically maize and sugarcane, which are not only expensive but have also created a food versus fuel dilemma. Alternatively, non-edible plants produced on non-arable lands offer a low-cost alternative without any direct or indirect competition with food or land (Ahmad et al., 2017a). Here, the problem is not the availability of the biomass, but rather the cost-effective and efficient retrieval of the energy stored in the biomass. Several processes have been developed to retrieve the biomass energy including direct combustion, thermochemical and biological conversion, where pyrolysis and biological fermentation are the cleanest methods to convert the biomass into valuable products. However, the latter is a tedious, expensive and time-consuming process, mainly due to the recalcitrant nature of the biomass. While, the thermal transformation of biomass into various products including solid, liquid and gasses often under an inert environment is called pyrolysis. Moreover, pyrolysis process leaves almost no waste, and all converted components can be used for one or another purpose ranging from energy (heat, bio-oil) through agricultural (char) and industrial chemicals (gases). However, the pyrolysis process depends upon various factors including nature of the biomass, particle size and temperature parameters. Hence, for an efficient conversion of any biomass, it is essential to understand its pyrolysis behavior to design an optimized pyrolytic process.

Thermogravimetric analyses performed under controlled conditions are practically feasible to understand the pyrolytic behavior and to determine the optimum pyrolytic conditions of any biomass (Di Blasi, 2009; Kow et al., 2014). The thermochemical conversion has dominance over biological processes because it has higher efficiency (Zhang et al., 2006). However, a clear understanding of the pyrolytic conditions is required for any biomass prior to feeding this biomass to any commercial thermal plant. Artificial Neural Networks (ANN) are

models which are developed based on the functionality of a human brain in which neurons transfer data from synapses on the way to axons through chemicals called neurotransmitters. Similarly, ANNs are composed of multiple neuron layers including input layers, hidden layers, and output layer to learn the relationship between them for further problem-solving approaches between experimental and predicted data (Kalogirou, 2003). Consequently, ANNs have been proven to be a useful tool to predict the reaction chemistry (Conesa et al., 2004; Yıldız et al., 2016) and has been employed on thermal data for estimation from several standpoints through training, validation and testing of experimental data (Chen et al., 2017; Uzun et al., 2017).

Previously, several grasses including Camel grass (Mehmood et al., 2017), Corn cobs, Miscanthus, wheat straw (Álvarez et al., 2016) and Sorghum weeds (Rezende and Richardson, 2017), along with microalgae (Maurya et al., 2016), red-peppers waste (Maia and de Morais, 2016) and rice-husk (Zhang et al., 2016) were previously studied for their bioenergy potential using thermogravimetric analyses. The Napier Grass is already being used to produce fuel on the commercial thermal plant (He et al., 2017). The present study was focused on understanding the pyrolytic behavior, reaction chemistry and bioenergy potential of *Typha latifolia* via thermogravimetric analyses for the very first time. *T. latifolia* occurs across the globe including Asia, Africa, Americas and Europe. It is a perennial grass produced on marginal lands and is a famous wetland species and can be grown in brackish or polluted water, hence is a low-cost biomass resource. While cultivating on polluted or brackish water, its bioremediatory action can remove pollutants developing a bitter taste making it unsuitable for food or feed. It has higher energy potential and can produce 25 units more energy when compared to fossil fuel (Ussiri and Lal, 2017). To date, there is no study available on pyrolytic behavior using Artificial Neural Network Approach of *T. latifolia*, studying the reaction mechanism of the thermal degradation. Generally, the reaction order model is considered as a suitable reaction mechanism of the biomass as it confirms its viability throughout the pyrolysis process. High precision thermogravimetric and kinetic analyses of devolatilization process (Trninić et al., 2012) are also applied in this study.

2. Materials and Methods

2.1 Elemental composition and proximate analyses

The biomass of *T. latifolia* was collected from soil affected by salinity which was being irrigated with underground brackish water. Collected sample was washed under a tap and left to dry in air for several days. Air dried biomass was crushed using a manual crusher and put into an oven for 48 h, and was grounded to get particles of size ranging from 150-200 µm. Sun dried crushed biomass was subjected to proximate analyses to determine volatile matter (VM %), ash (%) moisture content (%) using the standard methods as described in ASTM (E872-&82 2006, E871-82 2006, E1755-01 2007). The fixed carbon (FC %) was calculated using the equation: $FC\ (\%) = 100 - (ash\ content + VM + moisture)$. To determine the VM and moisture content, known mass was put in oven-dried at 380K in triplicate for 16-24 h to get a constant mass. The loss in mass reflected the moisture content. Similarly, known mass from the oven dried sample was put into pre-weighed ceramic crucibles in triplicate and left at 775K in a Muffle furnace for 3-4 h to get a constant mass. Where, loss in mass reflected the volatile matter (VM) and residual mass reflected the ash content. The composition of organic elements including Carbon (C), Hydrogen (H), Sulphur (S), Nitrogen (N) and Oxygen (O) in the sample was estimated by an elemental analyzer (Vario EL Cube, Germany). During analyses, the Argon (Ar) was used as a carrier gas.

The High Heating Value (HHV) indicates the amount of energy to be evolved from a biomass. However, the experimental procedures to determine the HHV (MJ kg^{-1}) are expensive and may give undesired experimental faults (Nhuchhen and Salam, 2012). Hence, previously several correlation models were developed to calculate HHV. Here, the most appropriate model established to date was used to calculate the HHV as described (Nhuchhen and Salam, 2012).

2.2 TGA-DSC Experiment

TGA-DSC analyses were performed using an STA-409, NETZSCH-Gerätebau GmbH, Germany. After calibration (as described in the instruction manual), almost ten mg (10) of milled biomass (150-200 µm particle size) was put into the alumina crucibles and constantly heated from ambient temperature to 1275 K. Where, constant heating at the rate of 10, 30 and 50 $Kmin^{-1}$ was used. An inert environment was maintained using the nitrogen gas flow (100 mL min^{-1}) into the reaction chamber.

2.3 ANN Model Development

An Artificial Neural Network (ANN) model was established to govern weight loss as output data, using heating rate and temperature as input variables. The feed-forward Levenberg-Marquardt back-propagation algorithm was selected in MATLAB® R2014b for data prediction. The model depicts the input, hidden and output layers of the multi-layer network. Two neurons were included in the input layer; heating rate and temperature. In contrast, the output layer had a single neuron, the temperature dependent weight loss. 1,021 data points were used in this analysis which were divided among the training (70%), validation (15%) and testing (15%) phases. The epoch number was set to 52 and 6 validation checks were applied. The Mean Square Error (MSE) function, as seen in Equation 1, was used as an error function to evaluate the performance of each phase. The network model was optimized based on the target (t) and output values (o), as expressed in Equation 2.

$$MSE = \frac{1}{n[\sum_{i=1}^{n}(\lambda_i - \beta_i)^2]} \quad (1)$$

where λ_i: experimental values; β_i: predicted values; n: number of data points

$$R^2 = 1 - \left[\frac{\sum_i (t_i - o_i)^2}{\sum_i (o_i)^2}\right] \quad (2)$$

2.4 Mathematical model development for thermogravimetric analyses

A mathematical model was derived from analyzing the data obtained from the TGA-DSC experiments. In isoconversional methods, the disintegration rate of the sample is depicted as:

$$\frac{d\alpha}{dt} = kf(\alpha) \quad (3)$$

Where;

$$\alpha = (m_o - m_t)/(m_o - m_\infty) \quad (4)$$

Here

m_o is the initial mass, m_t is change in the mass, and m_α is the residual mass

Using k , equation (3) was re-written as follows;

$$\frac{d\alpha}{dt} = A\,exp\left(-\frac{E}{RT}\right) f(\alpha) \quad (5)$$

Where

A is pre-exponential factor (s^{-1})

E is activation energy $\left(\frac{KJ}{mol}\right)$

T is temperature in Kelvin (K)

R is Universal gas constant $(8.314\frac{J}{K.mol})$

t is the time in sec

Later, the heating rate $\beta = \frac{dT}{dt}$ and the conversion function, $f(\alpha) = (1-\alpha)$ were intrudced by which following equation was obtained;

$$\frac{d\alpha}{dT} = \frac{A}{\beta} exp\left(-\frac{E}{RT}\right)(1-\alpha) \quad (6)$$

Then, equation (6) was integrated for the initial conditions, α = 0, at $T = T_0$, and after some mathematical manpulation, the following equation was obtained;

$$g(\alpha) = \int_0^\alpha d\alpha/(1-\alpha) = ART^2/\beta E\,[1 - 2RT/E]exp\,(-\frac{E}{RT}) \quad (7)$$

g is the integral conversion function.

Equation 7 was rearranged, as the quantity $2RT/E$ was negligible when compared with unity, hence it was ignored (Coats and Redfern, 1964), which resulted in following equation;

$$g(\alpha) = (ART^2/\beta E)exp(-E/RT) \quad (8)$$

2.5 Calculation of kinetic and thermodynamic parameters

Kinetic parameters of the pyrolysis reaction are vital to understanding the thermal degradation behavior of the sample under study. Here, these parameters were calculated using the isoconversional models as described by FWO (Flynn-Wall-Ozawa) and KAS (Kissenger-Akahira-Sunose) (Akahira and Sunose, 1969; Flynn and Wall, 1966; Ozawa, 1965). A model-fitting method named Coats-Redfern (Coats and Redfern, 1964) was used to describe the reaction mechanism which includes an order of reaction, diffusional, and the contracting geometry (White et al., 2011). Accordingly, activation energy could be determined by using $f(\alpha)$ OR $g(\alpha)$ that was further compared with the results found from KAS and FWO methods to predict the most accurate reation mechanism.

The equation 8 was rearranged after taking logarithm on both sides to get following equation;

$$\ln\left(\frac{\beta}{T^2}\right) = ln(AR/Eg(\alpha)) - E/RT \quad (9) \text{ KAS method}$$

Moreover, equation 6 was subjected to integration using the initial conditions, α = 0, at $T = T_0$. Later, Doyle's approximation was introduced followed by a few mathematical modifications (Doyle, 1961), which gave equation (10);

$$\ln(\beta) = ln(AE/Rg(\alpha)) - E/RT \quad (10) \text{ FWO method}$$

The Coats and Redfern (CR) Method relies on asymptotic approximation $\frac{2RT}{E} \rightarrow 0$, giving following equation;

$$\ln\left(\frac{g(\alpha)}{T^2}\right) = ln(AR/\beta E) - E/RT \quad (11) \text{ CR Method}$$

The left side of each equation (9, 10 and 11) was plotted (y-axis) against the inverse of pyrolysis temperature (x-axis), for selected conversion point (α) to calculate kinetic parameters. The conversion point (α) was used to calculate the pre-exponential factors ($A\,s^{-1}$) using the conversion points plotted between $\ln\left(\frac{\beta}{T^2}\right)$, $\ln(\beta)$ and $\ln\left(\frac{g(\alpha)}{T^2}\right)$ against 1/T which gave a straight line. The activation energy values were calculated from the slopes (E). Moreover, the

thermodynamic parameters including ΔH (enthalpy), ΔG (Gibbs free energy) and ΔS (entropy) were calculated as described previously (Kim et al., 2010; Xu and Chen, 2013).

$$A = [\beta . Eexp(E/RT_m)]/(RT_m^2\ ) \quad (12)$$

$$\Delta H = E - RT \quad (13)$$

$$\Delta G = E + RT_m \ln (K_B T_m/hA) \quad (14)$$

$$\Delta S = \Delta H - \Delta G/T_m \quad (15)$$

Where:

K_B Boltzmann Constant ($1.381 * 10^{-23}\ J/K$)

h Plank Constant ($6.626 * 10^{-34} Js$)

T_m DTG peak temperature, K

3 Results and Discussion

3.1 Physicochemical parameters

The *T. latifolia* biomass contained C, H, N, S, and O as 44.00%, 6.09, 2.45%, 0.34%, and 32.34%, respectively. The sample was shown to contain 71% volatile matter, 19.5% fixed carbon and 8.8% alkali. The lower nitrogen (<2.45%) and sulfur content (<0.34%) in the sample indicated that there is a lower risk of emission of toxic gases (NO_x, SO_x) from its pyrolysis. The range of volatile content (%) in the was shown to be within the range exhibited by the established bioenergy crops including *Miscanthus gigantus* and *Arduno donax* (Jeguirim et al., 2010).

The HHV indicates the amount of energy available from the biomass upon combustion. The estimated HHV of the sample was shown be 18.32 MJ kg^{-1} which is reasonably higher than the HHVs of several well-known energy crops including *A. donax* (Giant reed), *M. gigantus, Phalaris arundinacea* (Reed canarygrass), *Salix* spp. (Willow), Para grass and Camel grass, which had shown the HHVs as 17.2, 17.80, 16.30, 15.03 (Howaniec and Smolinski, 2011;

Jeguirim et al., 2010; Paulrud and Nilsson, 2001), 15.10 (Ahmad et al., 2017b), and 15.00 MJ kg^{-1} (Mehmood et al., 2017), respectively. The estimated HHV indicate the remarkable energy potential of the *T. latifolia* when compared to recognized bioenergy crops. However, the HHV of *T. latifolia* biomass was shown to be lower when compared to HHV of sweet sorghum, i.e. 20-25 MJ kg^{-1} (Monti et al., 2008; Yan et al., 2016).

3.2 Analyses of TG-DTG curves

Thermogravimetric analyses exhibit the loss in biomass in response to increasing reaction temperature. Where lost mass is converted into various products. The curves obtained during this analysis (TG-DTG curves) indicate the thermochemical conversion of the subjected biomass into solids, liquids and gaseous products (Maia and de Morais, 2016). For the sample under study, the curves showed typical trend of thermal degradation of lignocelluloses when compared to the TG-DTG curves (Fig. 1) found for Switchgrass, Cardoon leaves, Elephant grass, Camel grass, rice husk, and red pepper waste (Biney et al., 2015; Braga et al., 2014; Maia and de Morais, 2016; Mehmood et al., 2017; Xu and Chen, 2013).

The characteristic temperatures associated with the mass loss during thermal degradation, are shown in Tables 1 and 2. The rate of thermal conversion of the sample was shown to be increased with the increased heating rate (Tables 1 and 2). The thermal conversion of the sample was shown to comprise of three stages with two zones during stage-II. The first stage started from ambient temperature to 485-495 K for all heating rates, with the loss of 7.42-8.32 % in mass, which indicates the release of retained moisture content within intercellular spaces or intracellular compartments. The second stage ranged from 485-660 K taking all heating rates into account, where most of the mass loss occurred (i.e. 51%). This stage was shown to contain two zones for all heating rates, where zone-I occurred between 485-591 K while zone-II appeared between 568-660 K. The third stage occurs from 660-1275 K, where almost 17% of the total mass was lost. The biomass containing lesser that 10 % retained moisture, is considered feasible for combustion, which makes this sample suitable for pyrolysis and combustion (Braga et al., 2014). However, thermal transformation showed the typical pattern of lignocellulosic biomass.

Where, most of the thermal conversion happened during stage-II, indicating the degradation of hemicellulose, cellulose, and pectin where the typical temperature for their degradation ranges from 485K through 660 K (Xu and Chen, 2013). The temperature range associated with the third stage followed by the long tail reflects lignin degradation and char formation (Braga et al., 2014). Most of the thermal transformation happened up to 700 K where 58%-62% loss of the mass happened. Hence, the thermal conversion of the *T. latifolia* biomass into various products may be optimized within this temperature range, using lower heating rate in an energy efficient manner. These values indicated the advantage of using *T. latifolia* for pyrolysis and combustion, when compared to the previously studied biomass samples including rice husk, water hyacinth, and elephant grass (Biney et al., 2015; Braga et al., 2014; Huang et al., 2016). Biochar yields of 24.59, 25.45 and 23.67% were observed up to 660 K at three heating rates, which were comparable to the biochar yields obtained from the pyrolysis of straw (23.68%) and bran (25.17%) of rice plant (Xu & Chen, 2013), and lower than Para grass (31.5%) (Ahmad et al., 2017b), and Camel grass (30.46%) (Mehmood et al., 2017). These values indicated the appropriateness of the sample for biochar production.

3.3 Heat flow during pyrolysis reaction

The DSC curves showed a direct connection between the heating temperature and the flow of heat ($mWmg^{-1}$) because most of the pyrolysis reaction indicated an active reaction mechanism (Fig. 2). However, ending stages showed a decreasing heat flow. The reaction rate was steadily enhanced from ambient temperatures to 589, 754 and 799 K at 10, 30 and 50 $Kmin^{-1}$, respectively, which reflects exothermic reactions. These differences in heat flow may be due to the poor thermal conductivity of the biomass at various heating rates. The DSC curves started shifting towards x-axes at higher temperatures, which indicates the reaction to cease due to depletion of reactant (the biomass) or the change of reaction mechanism due to changing composition of the residual biomass. Because most of the volatiles were lost above 700 K, leading towards a different heat flow into the changing composition of the residual biomass. These curves exhibited parallel trend when compared to the DSC curves observed for bamboo leaves (Kow et al., 2016), the *Potamogeton crispus* and *Sargassum thunbergii*, where former is a freshwater plant and later is a marine macroalga (Li et al., 2012).

3.4 Kinetics and thermodynamic parameters

Figure 3 shows the linear fit plots to determine the activation energy values using KAS and FWO methods. These slopes and derived equations were used to calculate the conforming values of *E* and *A* as shown in Table 3. The average *E*-values were 184 kJ mol^{-1} and 182 kJ mol^{-1} as evaluated by both (KAS and FWO) methods. Moreover, a plot between *E*-values and conversion points (α) indicated that both methods have nearly same values at each conversion point. The relationship of activation energies, temperature and conversion points is described in Table 4. The observed range of *E* is lower than *E*-values (118-257 kJ mol^{-1}) of tobacco plant waste (Wu et al., 2015), rice husk (221-229 kJ mol^{-1}), cellulose (191 kJ mol^{-1}) and elephant grass (218-227 kJ mol^{-1}) (Braga et al., 2014; Sanchez-Jimenez et al., 2013) and this range was approximately same as Para grass (Ahmad et al., 2017b) and shown to be higher than switchgrass (Biney et al., 2015). This correspondence of *E*-values of *T. latifolia* makes it suitable for co-pyrolysis with several other biomass feedstocks.

The difference between the activation energy values and enthalpies reflects the likelihood of the pyrolysis reaction to occur. Where lower difference indicates that product formation would be favorable. A difference of ~5 kJ mol^{-1} was observed between the *E* and ΔH values that indicated that there is little potential energy barrier to achieve the product formation, reflecting that product formation would be easier to achieve (Vlaev et al., 2007). Moreover, pre-exponential factors (*A*-values) explain the reaction chemistry, which is critically important to know while optimizing the pyrolysis of biomass. While lower *A*-values ($<10^9$ s^{-1}) show largely a surface reaction. However, if the reaction is not surface dependent, then lower *A*-values also designate a closed complex. Alternatively, higher *A*-values ($\geq 10^9$ s^{-1}) show a simpler complex (Turmanova et al., 2008). For the sample under study, the *A*-values ranged from $5.53 \times 10^{10} - 3.02 \times 10^{15}$ s^{-1} and $7.61 \times 10^{09} - 7.93 \times 10^{15}$ s^{-1} as obtained from KAS and FWO methods, respectively (Table 3) that indicated the complexity of biomass. Moreover, *A*-values of sample were higher when compared to *A*-values of red-peppers waste (3.80×10^0 to 2.80×10^{12} s^{-1}), rice straw (1.70×10^{07} to 9.35×10^{12} s^{-1}), rice bran (1.00×10^{07} and 1.58×10^{10} s^{-1}) and were lower when compared to switchgrass (3.70×10^{03}-1.65×10^{21} s^{-1}) (Maia and de Morais, 2016). Gibbs free energy (ΔG) reflects the amount of energy which become available from that biomass upon pyrolysis. Here,

the ΔG values were shown to be ranging from 173-175 that are higher when compared with the ΔG values of the rice bran (167.17 kJ mol^{-1}), rice straw (164.59 kJ mol^{-1}) and waste from red-peppers (139.4 kJ mol^{-1}) (Maia and de Morais, 2016; Xu and Chen, 2013). It indicated that the pyrolysis of the *T. latifolia* will provide more energy when compared to the rice bran, rice straw and red-peppers waste.

3.5 Reaction mechanism of the pyrolysis

The CR method was devised on thermogravimetric data at three different heating rates to obtained *E*-values based on various reaction mechanisms (Table 5). Plots between $\ln\left(\frac{g(\alpha)}{T^2}\right)$ against 1/T were produced on various reaction mechanism functions as shown in Fig. 4. There were two regions formed based on conversion of the sample on three different heating rates. Region-I was defined when α ranged from $0.1 \leq \alpha \leq 0.4$ and Region-II was defined when α ranged from $0.4 \leq \alpha \leq 0.8$, where the major part of decomposition occurred. If the average activation energy values obtained from these mechanism functions at different heating rates are nearly equal to the energy values obtained from KAS and FWO methods, it shows this mechanism function should be the best-fit reaction of that region.

It was shown that in region-I the average *E* values are different in different reaction mechanism functions under three different heating rates. For reaction order model, the average *E* values of three heating rates ranged from 5.75 to 95.79 kJ mol^{-1}, whereas in diffusional stage these values ranged from 177.14 to 192.25 kJ mol^{-1} which were closest to the values obtained from KAS and FWO methods. It indicates that during the reactions displayed in Region-I, the diffusion played a key role (A. Khawam, 2006). In contraction geometry, the average *E*-values were too small and ranged from 88 to 91 kJ/mol. Similarly, in Region-II the average *E*-values depended upon 2^{nd} and 3^{rd} order reaction model and ranged from 116 to 200 kJ mol^{-1} which shows that *E*-values obtained from KAS and FWO methods are in between these values. Therefore, reaction order mechanism is classified as diffusion type followed by the 2^{nd} and 3^{rd} order reaction which is proportional to the concentration, total or residual amount of reactant(s) in a certain reaction (A. Khawam, 2006).

3.6 Prediction of pyrolytic behavior by ANN model

ANN model was applied to predict and validate the pyrolysis experiment at three different heating rates to simulate the predicted results with experimental data to further understand the pyrolytic behavior of *T. latifolia.* First, one hidden layer was created to have a simpler ANN model but three different breakdown stages resulted in sharp changes in data which complicated behavior of the sample. The best network performance was achieved with two hidden layers. Moreover, error distribution was analyzed at each step to ensure the accuracy of the network. The regression of each step was carried out during the optimization of the network that showed good correlation between targets and the output values, as shown in the Fig. 5. Moreover, the histogram error distribution diagram appears to be normally distributed for the major part of the obtained dataset. The R^2 value for the model fit at all stages appeared to be very close to 1, signifying a very good fit of the model to the experimental data (Fig. 5). Additionally, all these errors fall within a relatively narrow range; thus, indicating a good model fit. Here, 52 iterations were carried out by MATLAB and the best performance was observed at the 46th iteration with the minimum MSE (i.e. 0.53478). The obtained best performance results, as generated by MATLAB, are shown in Fig. 6. This finding indicates that ANN may be frequently applied to understand and envisage the pyrolysis of the biomass.

Conclusion

Major pyrolysis products of *T. latifolia* can be achieved at 485-660K. The E and ΔG values ranged from 182-184 kJmol^{-1} and 171-175 kJmol^{-1}, respectively. The HHV value (18.32 MJ kg^{-1}) was shown to be higher than several established energy crops. Moreover, best-fit plots were obtained by comparing experimental data with the predicted data points obtained from ANN simulation. The reaction mechanism showed the pyrolysis to contain two regions. Region-I ($0.1 \leq \alpha \leq 0.4$) and Region-II ($0.4 \leq \alpha \leq 0.8$). The best reaction model in Region-I was diffusion while in Region -II the best model was built on the 2nd to 3rd order reaction.

Acknowledgements

The financial support of Higher Education Commission Pakistan is highly appreciated.

Appendix-A: Supplementary data

This article contains supplementary information in its online version.

References

1. A. Khawam, D.R.F., 2006. Solid-state kinetic models: basics and mathematical fundamentals. J. Phys. Chem. B. 110, 17315–17328.
2. Ahmad, M.S., Mehmood, M.A., Ye, G., Al Ayed, O.S., Ibrahim, M., Rashid, U., Luo, H., Qadir, G., Nehdi, I.A. 2017a. Thermogravimetric analyses revealed the bioenergy potential of *Eulaliopsis binate*. J Therm. Anal. Calorim. DOI: 10.1007/s10973-017-6398-x.
3. Ahmad, M.S., Mehmood, M.A., Al Ayed, O.S., Ye, G., Luo, H., Ibrahim, M., Rashid, U., Nehdi, I.A., Qadir, G., 2017b. Kinetic analyses and pyrolytic behavior of Para grass (*Urochloa mutica*) for its bioenergy potential. Bioresour. Technol. 224, 708-713.
4. Akahira, T., Sunose, T., 1969. Transactions of Joint Convention of Four Electrical Institutes. 246.
5. Álvarez, A., Pizarro, C., García, R., Bueno, J.L., Lavín, A.G., 2016. Determination of kinetic parameters for biomass combustion. Bioresour. Technol. 216, 36-43.
6. Biney, P.O., Gyamerah, M., Shen, J., Menezes, B., 2015. Kinetics of the pyrolysis of arundo, sawdust, corn stover and switch grass biomass by thermogravimetric analysis using a multi-stage model. Bioresour. Technol. 179, 113-122.
7. Braga, R.M., Melo, D.M., Aquino, F.M., Freitas, J.C., Melo, M.A., Barros, J.M., Fontes, M.S., 2014. Characterization and comparative study of pyrolysis kinetics of the rice husk and the elephant grass. J. Therm. Anal. Calorim. 115, 1915-1920.
8. Chen, J., Liu, J., He, Y., Huang, L., Sun, S., Sun, J., Chang, K., Kuo, J., Huang, S., Ning, X., 2017. Investigation of co-combustion characteristics of sewage sludge and coffee grounds mixtures using thermogravimetric analysis coupled to artificial neural networks modeling. Bioresour. Technol. 225, 234-245.
9. Coats, A., Redfern, J., 1964. Kinetic parameters from thermogravimetric data. Nature 201, 68 – 69.
10. Conesa, J.A., Caballero, J.A., Reyes-Labarta, J.A., 2004. Artificial neural network for modelling thermal decompositions. J. Anal. Appl. Pyrol. 71, 343-352.

11. Di Blasi, C., 2009. Combustion and gasification rates of lignocellulosic chars. Prog. Energy Combust. Sci. 35, 121-140.
12. Doyle, C., 1961. Kinetic analysis of thermogravimetric data. J. Appl. Poly. Sci. 5, 285-292.
13. Edrisi, S.A., Abhilash, P., 2016. Exploring marginal and degraded lands for biomass and bioenergy production: An Indian scenario. Renew. Sustain. Energy Rev. 54, 1537-1551.
14. Flynn, J.H., Wall, L.A., 1966. A quick, direct method for the determination of activation energy from thermogravimetric data. J. Poly. Sci. B. 4, 323-328.
15. He, C.-R., Kuo, Y.-Y., Li, S.-Y., 2017. Lignocellulosic butanol production from Napier grass using semi-simultaneous saccharification fermentation. Bioresour. Technol. 231, 101-108.
16. Howaniec, N., Smolinski, A., 2011. Steam gasification of energy crops of high cultivation potential in Poland to hydrogen-rich gas. Int. J. Hydro. Energy 36, 2038-2043.
17. Huang, L., Liu, J., He, Y., Sun, S., Chen, J., Sun, J., Chang, K., Kuo, J., 2016. Thermodynamics and kinetics parameters of co-combustion between sewage sludge and water hyacinth in CO_2/O_2 atmosphere as biomass to solid biofuel. Bioresour. Technol. 218, 631-642.
18. Jeguirim, M., Dorge, S., Trouve, G., 2010. Thermogravimetric analysis and emission characteristics of two energy crops in air atmosphere: *Arundo donax* and *Miscanthus giganthus*. Bioresour. Technol. 101, 788-793.
19. Kalogirou, S.A., 2003. Artificial intelligence for the modeling and control of combustion processes: a review. Prog. Energy Combust. Sci. 29, 515-566.
20. Kim, Y.S., Kim, Y.S., Kim, S.H., 2010. Investigation of thermodynamic parameters in the thermal decomposition of plastic waste– waste lube oil compounds. Environ. Sci. Technol. 44, 5313-5317.
21. Kow, K-W., Yusoff, R., Abul Aziz, A.R., Abdullah, E.C. 2014. Characterisation of bio-silica synthesised from cogon grass (*Imperata cylindrica*). Powder Technol. 254, 206-213.

22. Kow, K-W., Yusoff, R., Abul Aziz, A.R., Abdullah, E.C. 2016. Determination of kinetic parameters for thermal decomposition of bamboo leaf to extract bio-silica. Energ. Source Part A. 38, 3249-3254.
23. Li, D., Chen, L., Chen, S., Zhang, X., Chen, F., Ye, N., 2012. Comparative evaluation of the pyrolytic and kinetic characteristics of a macroalga (*Sargassum thunbergii*) and a freshwater plant (*Potamogeton crispus*). Fuel. 96, 185-191.
24. Maia, A.A.D., de Morais, L.C., 2016. Kinetic parameters of red pepper waste as biomass to solid biofuel. Bioresour. Technol. 204, 157-163.
25. Maurya, R., Ghosh, T., Saravaia, H., Paliwal, C., Ghosh, A., Mishra, S., 2016. Non-isothermal pyrolysis of de-oiled microalgal biomass: Kinetics and evolved gas analysis. Bioresour. Technol. 221, 251-261.
26. Mehmood, M.A., Ye, G., Luo, H., Liu, C., Malik, S., Afzal, I., Xu, J., Ahmad, M.S., 2017. Pyrolysis and kinetic analyses of Camel grass (*Cymbopogon schoenanthus*) for bioenergy. Bioresour. Technol. 228, 18-24.
27. Monti, A., Di Virgilio, N., Venturi, G., 2008. Mineral composition and ash content of six major energy crops. Biomass Bioener. 32, 216-223.
28. Nhuchhen, D.R., Salam, P.A., 2012. Estimation of higher heating value of biomass from proximate analysis: A new approach. Fuel. 99, 55-63.
29. Ozawa, T., 1965. A new method of analyzing thermogravimetric data. Bull. Chem. Soc. Jpn. 38, 1881-1886.
30. Paulrud, S., Nilsson, C., 2001. Briquetting and combustion of spring-harvested reed canary-grass: effect of fuel composition. Biomass Bioener. 20, 25-35.
31. Rezende, M.L., Richardson, J.W., 2017. Risk analysis of using sweet sorghum for ethanol production in southeastern Brazil. Biomass Bioener. 97, 100-107.
32. Sanchez-Jimenez, P.E., Perez-Maqueda, L.A., Pereon, A., Criado, J.M., 2013. Generalized master plots as a straightforward approach for determining the kinetic model: the case of cellulose pyrolysis. Thermochimica Acta 552, 54-59.
33. Trninić, M., Wang, L., Várhegyi, G., Grønli, M., Skreiberg, Ø., 2012. Kinetics of corncob pyrolysis. Energy Fuels 26, 2005-2013.

34. Turmanova, S.C., Genieva, S., Dimitrova, A., Vlaev, L., 2008. Non-isothermal degradation kinetics of filled with rise husk ash polypropene composites. Exp. Poly. Lett. 2, 133-146.
35. Ussiri, D.A.N., Lal, R., 2017. The Role of Bioenergy in Mitigating Climate Change Carbon Sequestration for Climate Change Mitigation and Adaptation. Springer International Publishing, Cham, pp. 433-495.
36. Uzun, H., Yıldız, Z., Goldfarb, J.L., Ceylan, S., 2017. Improved prediction of higher heating value of biomass using an artificial neural network model based on proximate analysis. Bioresour. Technol. 234, 122-130.
37. Vlaev, L., Georgieva, V., Genieva, S., 2007. Products and kinetics of non-isothermal decomposition of vanadium (IV) oxide compounds. J. Therm. Anal. Calorim. 88, 805-812.
38. White, J.E., Catallo, W.J., Legendre, B.L., 2011. Biomass pyrolysis kinetics: A comparative critical review with relevant agricultural residue case studies. J. Anal. Appl. Pyrol. 91, 1-33.
39. Wu, W., Mei, Y., Zhang, L., Liu, R., Cai, J., 2015. Kinetics and reaction chemistry of pyrolysis and combustion of tobacco waste. Fuel 156, 71-80.
40. Xu, Y., Chen, B., 2013. Investigation of thermodynamic parameters in the pyrolysis conversion of biomass and manure to biochars using thermogravimetric analysis. Bioresour. Technol. 146, 485-493.
41. Yan, H.-L., Zong, Z.-M., Li, Z.-K., Kong, J., Zheng, Q.-X., Li, Y., Wei, X.-Y., 2016. Sweet sorghum stalk liquefaction in supercritical methanol: Effects of operating conditions on product yields and molecular composition of soluble fraction. Fuel Process. Technol. http://dx.doi.org/10.1016/j.fuproc.2016.02.011.
42. Yıldız, Z., Uzun, H., Ceylan, S., Topcu, Y., 2016. Application of artificial neural networks to co-combustion of hazelnut husk–lignite coal blends. Bioresour. Technol. 200, 42-47.
43. Zhang, S., Dong, Q., Zhang, L., Xiong, Y., 2016. Effects of water washing and torrefaction on the pyrolysis behavior and kinetics of rice husk through TGA and Py-GC/MS. Bioresour. Technol. 199, 352-361.

44. Zhang, X., Xu, M., Sun, R., Sun, L., 2006. Study on biomass pyrolysis kinetics. J. Eng. Gas Turbines Power 128, 493-496.

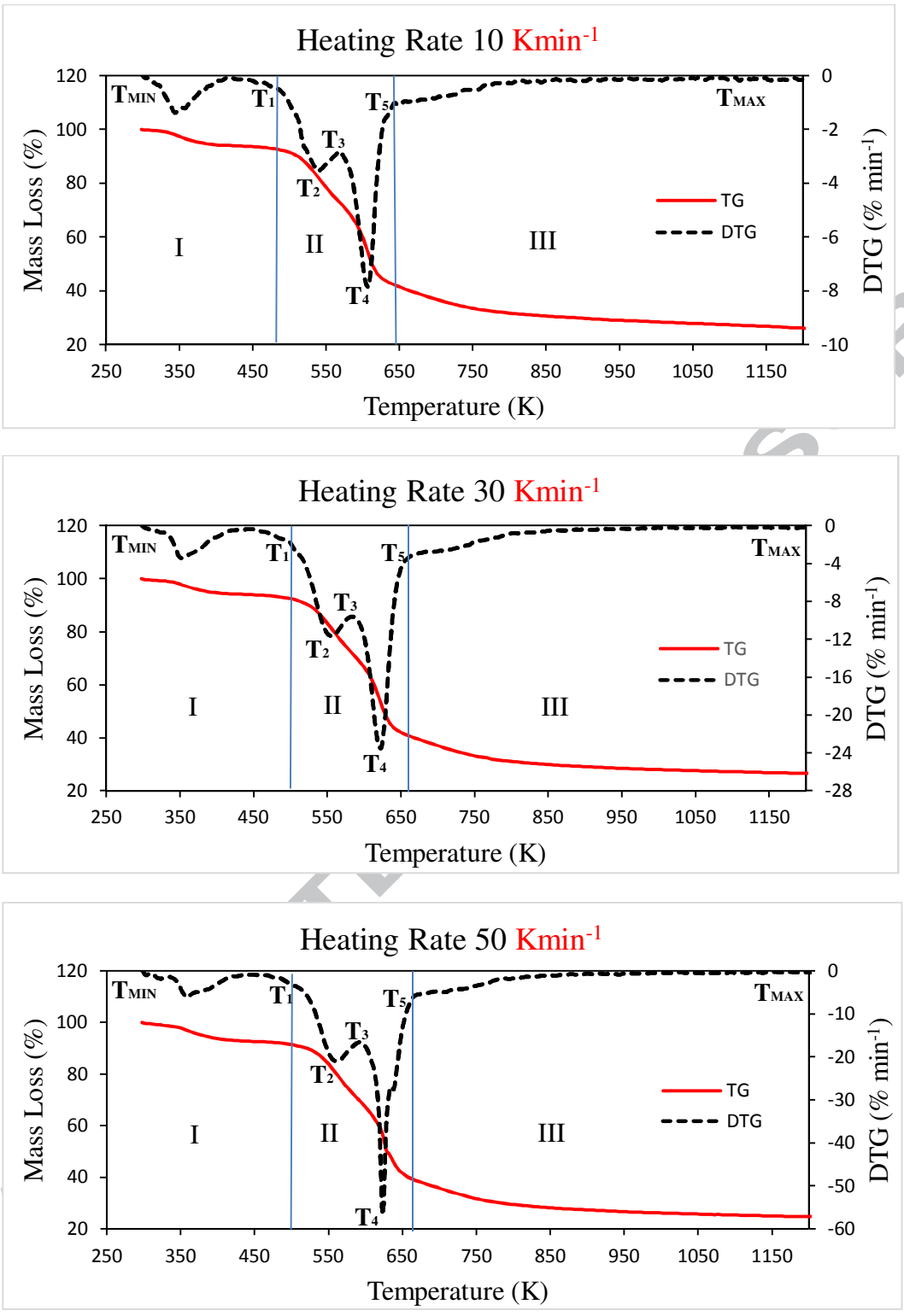

Fig. 1 TG-DTG curves indicating percent mass loss of *Typha latifolia*

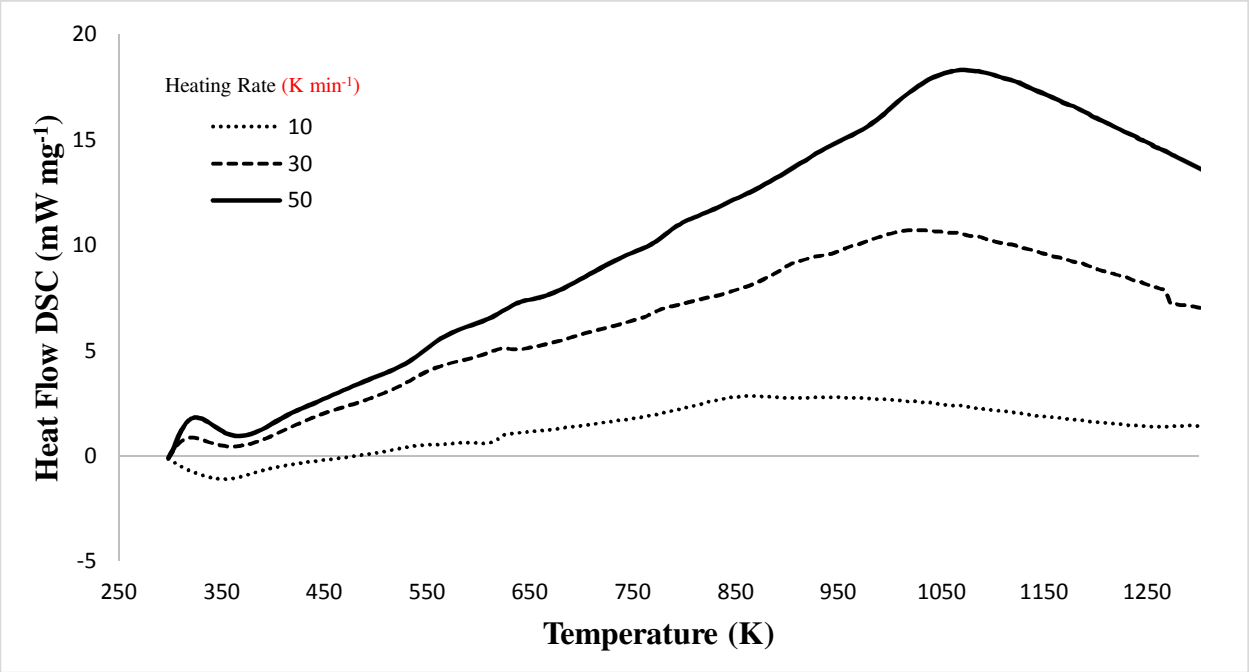

Fig. 2 DSC curves indicating heat flow across the biomass

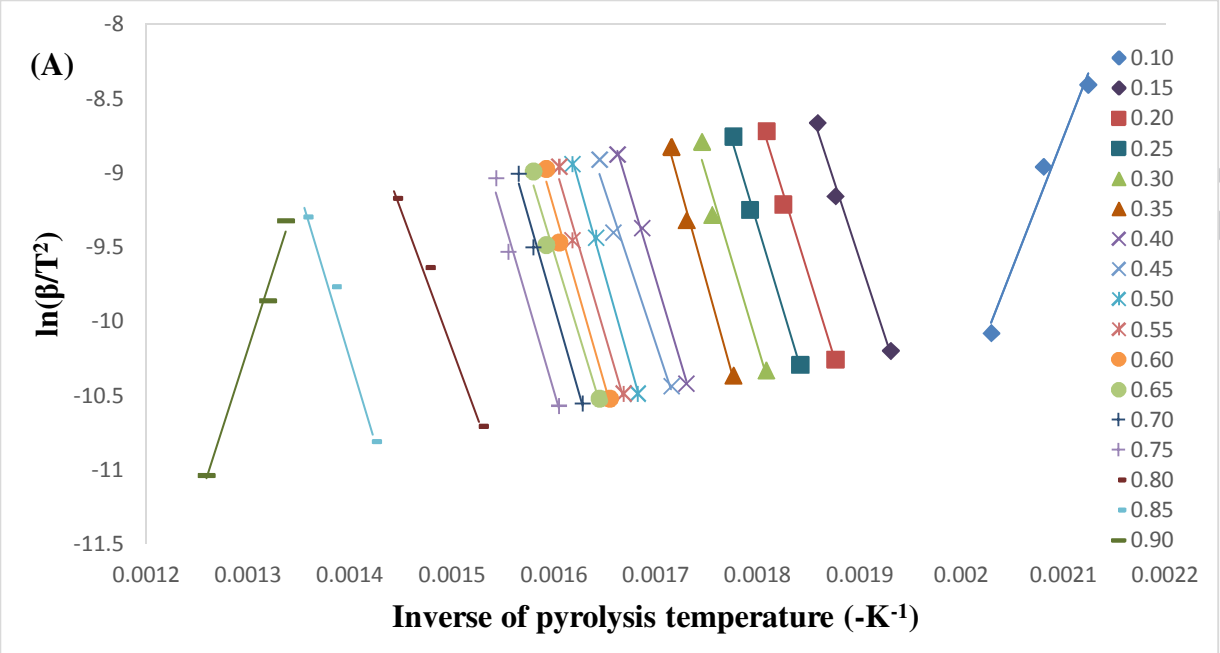

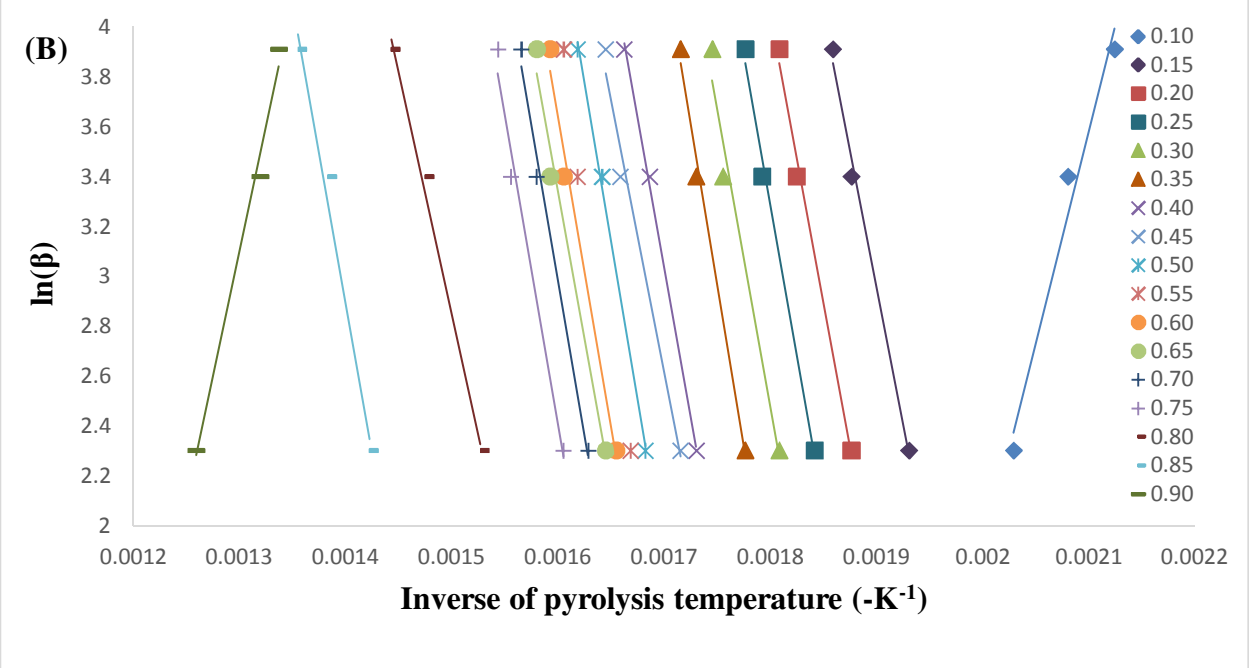

Fig.3 Linear fit plots to determine the activation energy values using KAS and FWO methods

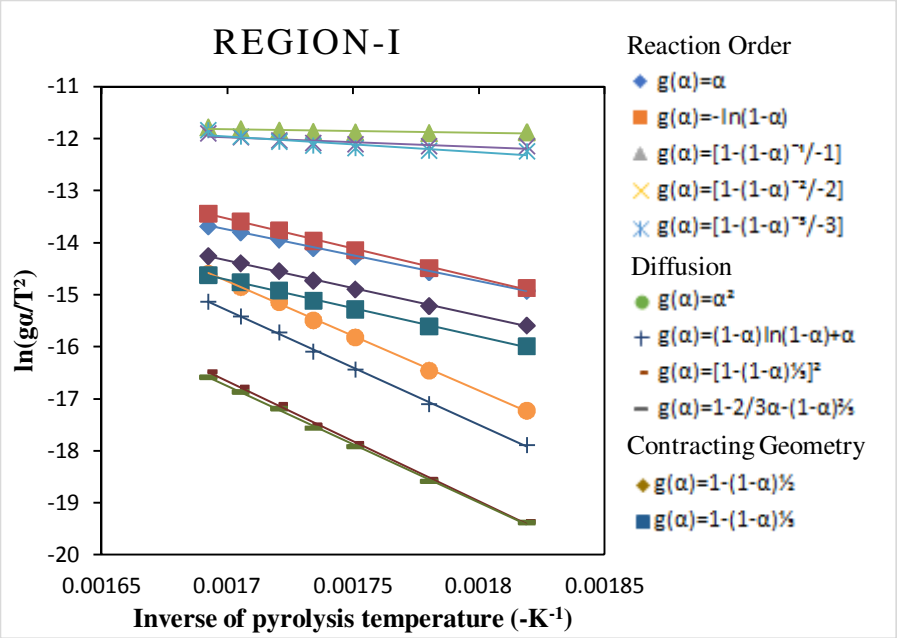

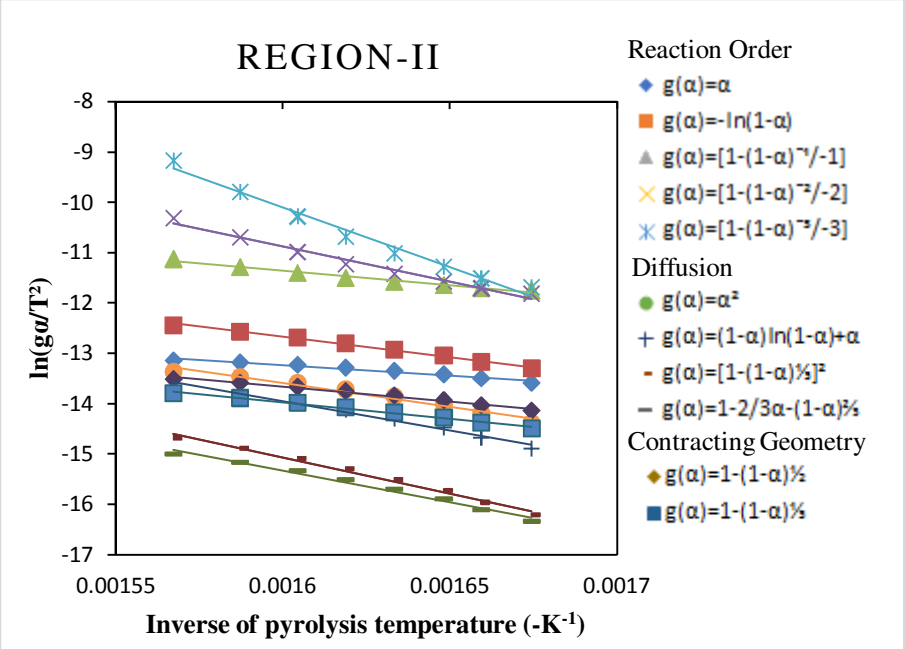

Fig.4 CR Plots of for pyrolysis of *T. latifolia.* Region-I ($.1 \leq \alpha \leq .4$) and Region-II ($.4 \leq \alpha \leq .8$)

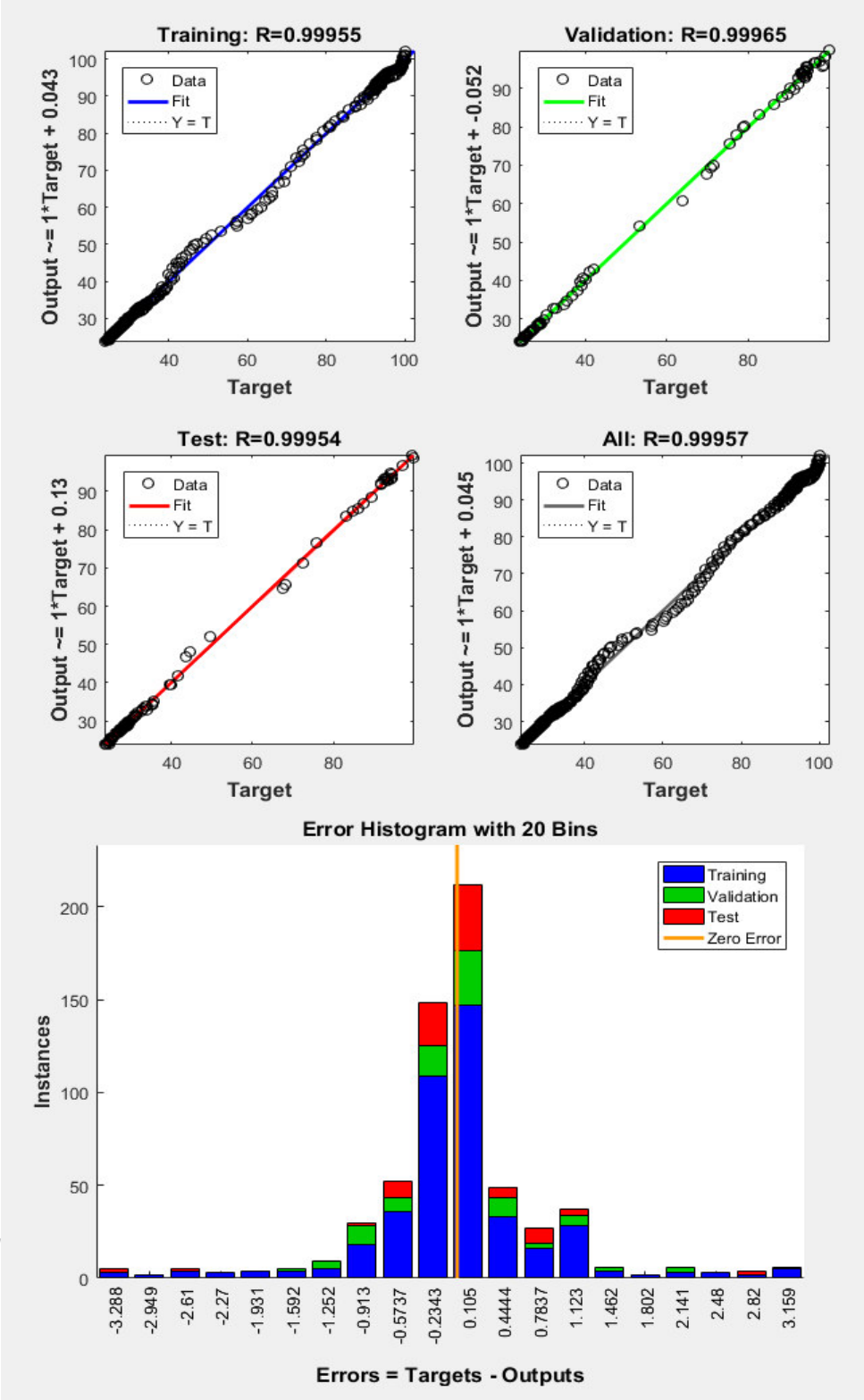

Fig.5 Regression of train, validate and testing steps together with histogram diagram

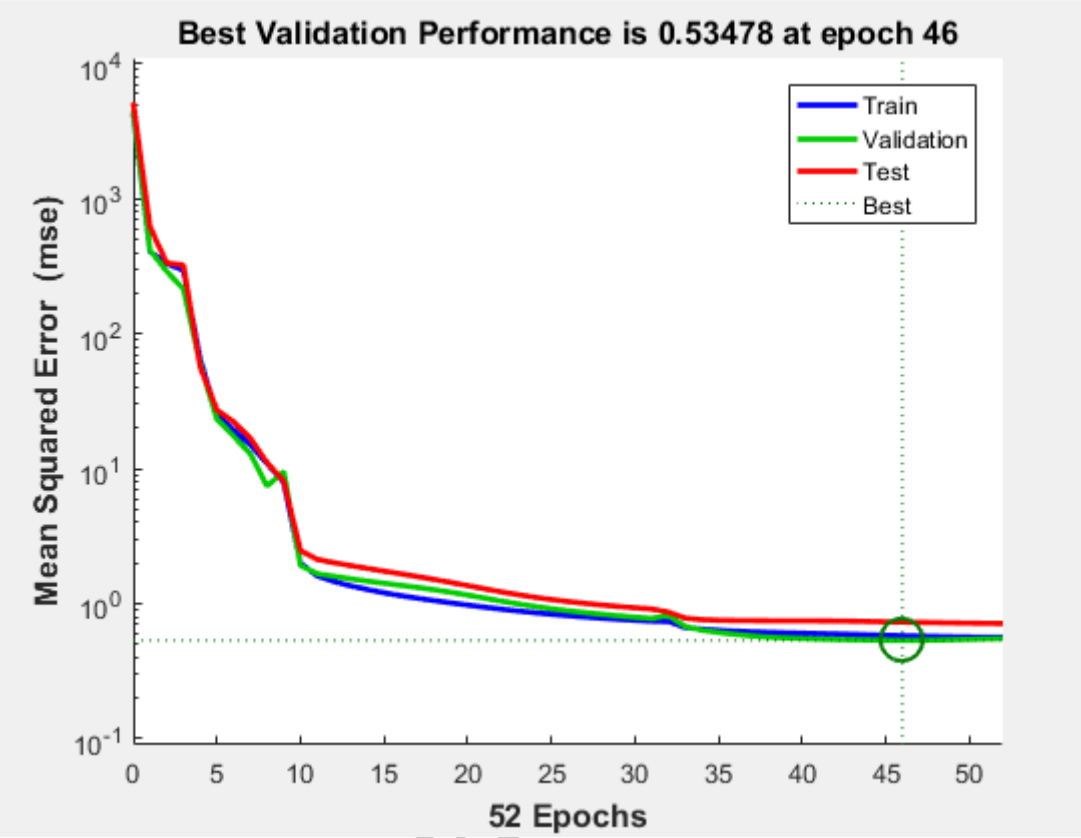

Fig.6 Best performance Mean Square Error (MSE) vs Targets

Table 1 Characteristic temperatures associated with the mass loss

Heating rate ($Kmin^{-1}$)	Temperature (K)						
	T_{min}	T_1	T_2	T_3	T_4	T_5	T_{max}
10	298	485	538	568	606	644	1300
30		499	555	584	621	654	
50		495	556	591	623	660	

Table 2

Mass loss during different stages of decomposition with increasing temperature

Stages		Temperature	Heating rate ($Kmin^{-1}$)		
			10	**30**	**50**
Stage-I, WL (%)		T_{min}-T_1	7.45	7.46	8.32
Stage-II, WL (%)	Region-I	T_1-T_3	19.65	20.58	21.62
	Region-II	T_3-T_5	30.83	30.30	30.17
Stage-III, WL (%)		T_5-T_{max}	17.48	16.21	16.22
Final residues at 1075-1275K (%)		--	24.59	25.45	23.67

Table 3 Kinetic and thermodynamics parameters of *T. latifolia*

α	E_a kJmol^{-1}	R^2	ΔH kJmol^{-1}	A s^{-1}	ΔG kJmol^{-1}	ΔS Jmol^{-1}	E_a kJmol^{-1}	R^2	ΔH kJmol^{-1}	A s^{-1}	ΔG kJmol^{-1}	ΔS Jmol^{-1}
KAS method							**FWO method**					
0.1	147.20	0.99	142.04	5.53E+10	175.37	-53.67	134.78	0.99	129.62	7.61E+09	173.18	-70.16
0.15	173.56	0.98	168.40	1.08E+13	174.51	-9.85	173.31	0.99	168.15	1.71E+13	171.88	-6.01
0.2	183.84	0.98	178.68	8.34E+13	174.22	7.18	183.32	0.99	178.16	1.25E+14	171.59	10.57
0.25	190.85	0.98	185.68	3.37E+14	174.02	18.78	190.15	0.99	184.98	4.88E+14	171.41	21.87
0.3	189.93	0.99	184.76	2.80E+14	174.05	17.25	189.12	0.99	183.96	3.98E+14	171.43	20.17
0.35	201.89	0.99	196.73	3.02E+15	173.73	37.02	204.18	0.99	199.01	7.93E+15	171.04	45.05
0.4	185.30	0.99	180.14	1.12E+14	174.18	9.60	188.97	0.99	183.81	3.86E+14	171.44	19.92
0.45	171.24	0.99	166.07	6.77E+12	174.58	-13.71	172.40	0.98	167.24	1.42E+13	171.91	-7.52
0.5	201.89	0.99	196.73	3.02E+15	173.73	37.02	200.18	0.99	195.02	3.59E+15	171.14	38.46
0.55	193.13	0.99	187.96	5.30E+14	173.96	22.54	196.03	0.99	190.87	1.57E+15	171.25	31.60
0.6	197.73	0.99	192.57	1.32E+15	173.84	30.16	196.55	0.99	191.39	1.74E+15	171.23	32.45
0.65	186.65	0.99	181.49	1.46E+14	174.14	11.83	187.22	0.99	182.06	2.73E+14	171.49	17.02
0.7	198.37	0.99	193.21	1.50E+15	173.82	31.21	196.39	0.99	191.23	1.69E+15	171.24	32.19
0.75	196.05	0.98	190.89	9.48E+14	173.89	27.38	190.75	0.98	185.58	5.50E+14	171.39	22.86
0.8	153.94	0.99	148.78	2.14E+11	175.13	-42.44	153.00	0.99	147.84	2.95E+11	172.53	-39.76
0.85	188.69	0.99	183.53	2.19E+14	174.08	15.22	190.75	0.99	185.58	5.50E+14	171.39	22.86
0.9	177.61	0.99	172.45	2.41E+13	174.40	-3.13	158.36	0.99	153.20	8.62E+11	172.35	-30.84
Avg.	**184.58**	**0.99**	**179.42**	**--**	**174.22**	**--**	**182.67**	**0.99**	**177.51**	**--**	**171.64**	**--**

Table 4 Relationship between conversion (α), pyrolysis temperature (*T*) and activation energies (*E*)

Conversion range (α)	Temperature range (K)	Reactions	Activation energy (*E*)
$\alpha \leq 0.1$	273-485	Release of retained water moisture and degradation of small and simple sugar molecules	Increased from starting point to 147 kJ mol^{-1}
$0.1 \leq \alpha \leq 0.4$	485-591	Thermal conversion of cellulose and pectin	Increased from 147 to 185 kJ mol^{-1}
$0.4 \leq \alpha \leq 0.8$	591-660	Degradation of hemicellulose and lignin	Increased from 185 to 196 kJ mol^{-1}
$0.1 \leq \alpha \leq 1.0$	660-1200	Residual lignin decomposition and formation of char	Decreased from 196 to 177 kJ mol^{-1}

Table 5: Activation Energy values and reaction mechanism based on Coats-Redfern method

Region	Reaction Model	g(α)	10 Kmin^{-1}		30 Kmin^{-1}		50 Kmin^{-1}		Average values	
			E_a kJmol^{-1}	R^2	E_a kJmol^{-1}	R^2	E_a kJmol^{-1}	R^2	E_a kJmol^{-1}	R^2
I	**Reaction Order**									
	Zero-order *(F0)*	α	5.52	0.99	5.67	0.98	6.05	0.97	5.75	0.98
	First-order *(F1)*	$-\ln(1-\alpha)$	82.50	0.97	82.81	0.99	83.46	0.99	82.92	0.98
	nth-order *(Fn)*	$[1-(1-\alpha)^{-1}/-1]$	94.97	0.99	95.21	0.95	97.18	0.96	95.79	0.97
		$[1-(1-\alpha)^{-2}/-2]$	15.31	0.88	17.23	0.98	18.54	0.96	17.03	0.94
		$[1-(1-\alpha)^{-3}/-3]$	25.55	0.96	27.67	0.99	29.33	0.98	27.52	0.98
	Diffusion									
	1-D	α^2	174.48	0.99	177.70	0.99	179.23	0.99	177.14	0.99
	2-D	$(1-\alpha)ln(1-\alpha)+\alpha$	182.38	0.99	183.21	0.98	185.93	0.99	183.84	0.99
	3-D *(Jander)*	$[1-(1-\alpha)^{⅓}]^2$	190.82	0.98	191.83	0.99	194.11	0.98	192.25	0.98
	3-D *(Ginstling-Brounshtein)*	$1-2/3\alpha-(1-\alpha)^{⅔}$	185.19	0.96	186.22	0.97	188.73	0.97	186.71	0.97
	Contracting Geometry									
	Cont. Area	$1-(1-\alpha)^{½}$	88.58	0.99	90.01	0.90	87.51	0.98	88.70	0.96
	Cont. Volume	$1-(1-\alpha)^{⅓}$	90.67	0.84	91.41	0.89	93.85	0.88	91.98	0.87
II	**Reaction Order**									
	Zero-order *(F0)*	α	34.69	0.95	35.61	0.96	36.59	0.96	35.63	0.96
	First-order *(F1)*	$-ln(1-\alpha)$	67.27	0.97	68.34	0.97	70.37	0.98	68.66	0.97
	nth-order *(Fn)*	$[1-(1-\alpha)^{-1}/-1]$	48.61	0.98	50.51	0.98	49.40	0.99	49.51	0.98
		$[1-(1-\alpha)^{-2}/-2]$	116.59	0.99	115.43	0.99	118.49	0.99	116.84	0.99
		$[1-(1-\alpha)^{-3}/-3]$	197.37	0.96	200.71	0.98	202.51	0.97	200.20	0.97
	Diffusion									
	1-D	α^2	79.64	0.99	81.45	0.99	83.83	0.98	80.97	0.99
	2-D	$(1-\alpha)ln(1-\alpha)+\alpha$	97.13	0.94	98.91	0.96	100.40	0.93	98.81	0.94
	3-D *(Jander)*	$[1-(1-\alpha)^{⅓}]^2$	120.01	0.81	124.23	0.84	127.82	0.80	124.02	0.82
	3-D *(Ginstling-Brounshtein)*	$1-2/3\alpha-(1-\alpha)^{⅔}$	104.66	0.99	108.55	0.99	110.17	0.99	107.79	0.99
	Contracting Geometry									
	Cont. Area	$1-(1-\alpha)^{½}$	49.26	0.99	51.12	0.89	54.32	0.92	51.57	0.93
	Cont. Volume	$1-(1-\alpha)^{⅓}$	55.68	0.79	58.59	0.76	61.48	0.72	58.58	0.76

- The *Typha latifolia* offers low-cost biomass from poor soils across the globe
- Its biomass was subjected to pyrolysis and thermogravimetric study
- Pyrolytic behavior and reaction mechanism is described
- The biomass has bioenergy potential comparable to well-known bioenergy crops